PNAS RESEARCH ARTICLE | ENGINEERING

Molecularly confined hydration in thermoresponsive hydrogels for efficient atmospheric water harvesting

Weixin Guan[a,1], Yaxuan Zhao[a,1], Chuxin Lei[a], and Guihua Yu[a,2]

Edited by Rodney D. Priestley, Princeton University, Princeton, NJ; received May 28, 2023; accepted August 7, 2023 by Editorial Board Member Pablo G. Debenedetti

Water scarcity is a pressing global issue, requiring innovative solutions such as atmospheric water harvesting (AWH), which captures moisture from the air to provide potable water to many water-stressed areas. Thermoresponsive hydrogels, a class of temperature-sensitive polymers, demonstrate potential for AWH as matrices for hygroscopic components like salts predominantly due to their relatively energy-efficient desorption properties compared to other sorbents. However, challenges such as limited swelling capacity due to the salting-out effect and difficulty in more complete water release hinder the effectiveness of conventional hydrogel sorbents. To overcome these limitations, we introduce molecularly confined hydration in thermoresponsive hydrogels by employing a bifunctional polymeric network composed of hygroscopic zwitterionic moieties and thermoresponsive moieties. Here, we show that this approach ensures stable water uptake, enables water release at relatively low temperatures, and exhibits rapid sorption–desorption kinetics. Furthermore, by incorporating photothermal absorbers, the sorbent can achieve solar-driven AWH with comparable water release performance. This work advances the design of AWH sorbents by introducing molecularly confined hydration in thermoresponsive hydrogels, leading to a more efficient and sustainable approach to water harvesting. Our findings offer a potential solution for advanced sorbent design with comprehensive performance to mitigate the freshwater crisis.

atmospheric water harvesting | hydrogel | desorption | hydration

Significance

With increasing global demand for freshwater and the concurrent dwindling of traditional water resources, it's imperative to explore sustainable alternatives for water supply. Atmospheric water harvesting (AWH), a potential solution, faces challenges due to the energy-intensive release of captured water. Addressing this issue, our study introduces the concept of molecularly confined hydration in thermoresponsive hydrogels, enabling more efficient water release at lower temperatures. This technique, when coupled with photothermal absorbers, harnesses solar energy, bolstering the sustainability of AWH. This advancement contributes to our understanding of hydrogel design for AWH and signifies a crucial step in the global efforts to mitigate the intensifying water scarcity crisis.

Addressing the escalating global challenge of limited access to potable water necessitates the exploration of more abundant water sources and the advancement of innovative water production methods (1, 2). In contrast to established water treatment techniques, such as seawater desalination, atmospheric water harvesting (AWH) has emerged as a decentralized approach, providing considerable potential for domestic implementation, regardless of geographical and hydraulic limitations (3, 4). Sorbent-based AWH (SAWH) exhibits the unique advantage of versatile functionality across diverse relative humidity (RH) levels, retaining efficacy even at levels as low as 15% RH (5–13). In a practical SAWH process, several key steps are typically involved, including the elimination of dirt and dust from the moisture flow, sorbent-mediated water production via sorption-desorption cycles, and subsequent water collection, with potential purification if necessary. Notably, the characteristics of the AWH sorbent exert a substantial influence on both the overall water yield and the energy consumption associated with the process (Fig. 1*A*).

Considerable efforts have been made to investigate cutting-edge AWH sorbents exhibiting high water uptake, rapid sorption-desorption kinetics, and energy-efficient water release (14, 15). Among a plethora of materials, polymeric hydrogels have attracted significant attention as a promising class of candidates, due to their remarkable water retention capacity and the ability to modulate desorption temperatures through distinct polymer–water interactions (16–18). Thermoresponsive hydrogels represent a subclass of hydrogels that undergo phase transitions in response to temperature fluctuations (19, 20). Specifically, hydrogels exhibiting lower critical solution temperatures (LCST), such as poly(N-isopropylacrylamide) (PNIPAM) (21, 22), have been utilized as AWH sorbents, as their characteristic hydrophilic-to-hydrophobic transition at temperatures exceeding the LCST facilitates water release at the molecular level (11, 17, 23, 24) (*SI Appendix*, S2.1).

To enhance the hygroscopic performance of thermoresponsive hydrogel sorbents, particularly under low RH conditions, the integration of hygroscopic salts such as lithium chloride (LiCl) and calcium chloride ($CaCl_2$) into the hydrogel matrix can be employed to develop composite sorbents with improved moisture absorption capabilities (24, 25). Salts will liquefy the adsorbed vapor through deliquescence, while the hydrogel network serves as a molecular reservoir for storing liquid water (18, 26). However, such composite sorbents may risk salt leakage at elevated RH due to uncontrolled deliquescence and insufficient salt confinement and may suffer from poor swelling capacity caused by the salting-out effect with high salt content (27, 28), which can deteriorate sorbent performance and narrow the range of

Author affiliations: [a]Materials Science and Engineering Program and Walker Department of Mechanical Engineering, The University of Texas at Austin, Austin, TX 78712

Author contributions: G.Y. designed research; W.G., Y.Z., and C.L. performed research; W.G., Y.Z., C.L., and G.Y. analyzed data; and W.G., Y.Z., and G.Y. wrote the paper.

The authors declare no competing interest.

This article is a PNAS Direct Submission. R.D.P. is a guest editor invited by the Editorial Board.

Copyright © 2023 the Author(s). Published by PNAS. This article is distributed under Creative Commons Attribution-NonCommercial-NoDerivatives License 4.0 (CC BY-NC-ND).

[1]W.G. and Y.Z. contributed equally to this work.

[2]To whom correspondence may be addressed. Email: ghyu@austin.utexas.edu.

This article contains supporting information online at https://www.pnas.org/lookup/suppl/doi:10.1073/pnas.2308969120/-/DCSupplemental.

Published September 11, 2023.

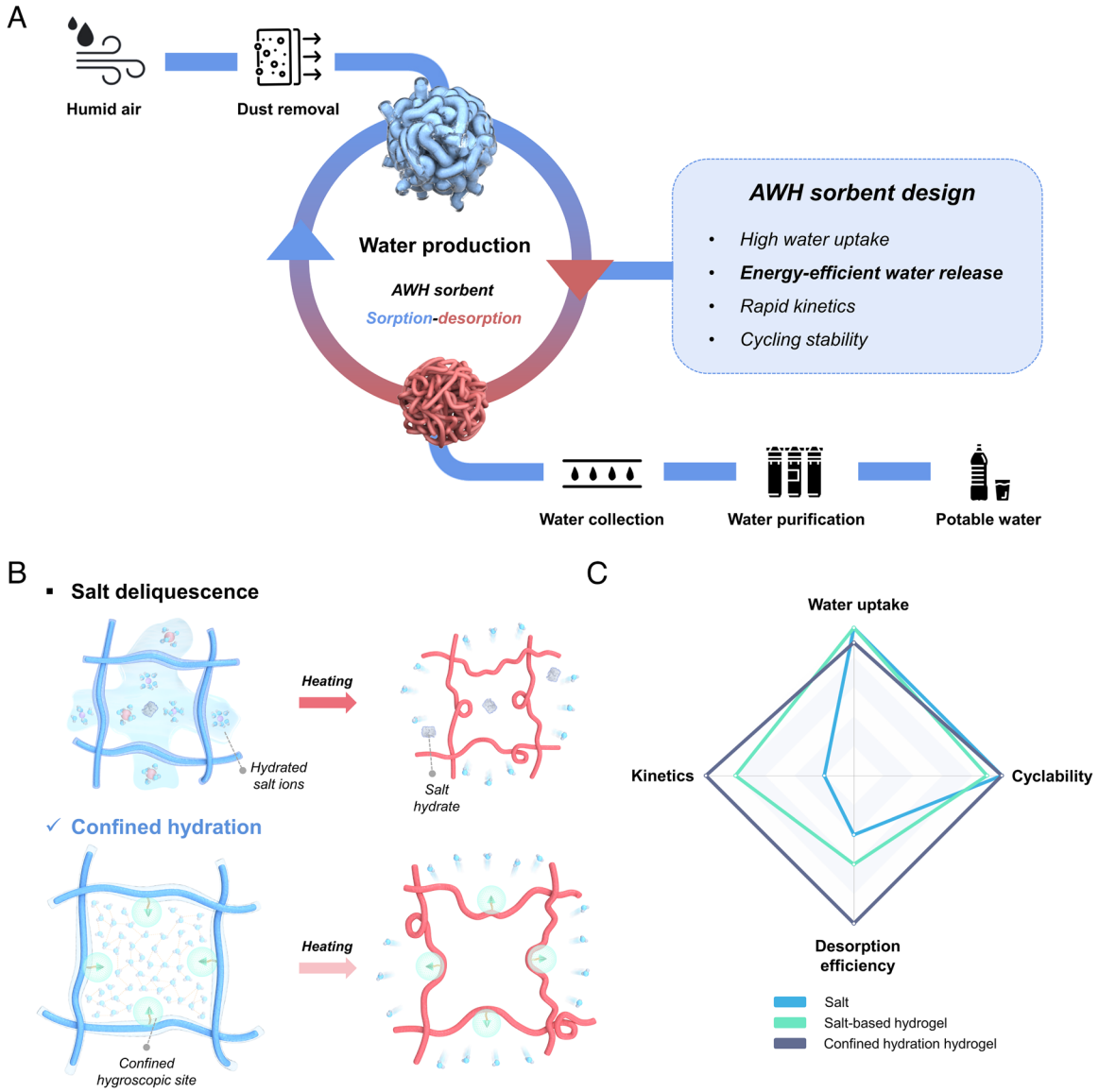

Fig. 1. AWH process and design rationale of AWH sorbents. (*A*) Illustration of a typical SAWH process. (*B*) Schematic representation of two moisture capture mechanisms: 1) Salt Deliquescence—a three-step process involving hygroscopic salts, including chemisorption, crystallization, and deliquescence, which requires elevated temperatures for complete desorption of salt hydrates; 2) Confined Hydration—molecularly confined hygroscopic sites enable water capture within the molecular mesh, allowing for water release at lower temperatures due to conformational changes in the thermoresponsive gel network without the involvement of crystal hydrates. (*C*) Qualitative comparison of salt-contained sorbents, highlighting key performance factors for AWH sorbents.

applicable scenarios. Moreover, higher temperatures are typically required for more complete water desorption, as aggregated salt hydrates necessitate considerable activation energy for decomposition (29, 30). Alternatively, the swelling capacity could be preserved under controlled water capture if hygroscopic ions are immobilized within a confined domain. Moreover, the potential reduction in energy consumption during desorption could be attained without the formation of aggregated crystal hydrates, given the limited mobility of ions. Herein, we propose a concept of confined hydration in thermoresponsive hydrogels for energy-efficient AWH (Fig. 1*B*). The confined hygroscopic sites attached to the polymer chain can largely immobilize salt ions, enabling confined water networking and hydrogel swelling within the molecular mesh rather than uncontrolled salt liquefaction. Upon mild heating, the disintegration of the water molecule network and subsequent water escape is facilitated by the conformational change of the thermoresponsive gel matrix.

In this study, molecularly confined hydration in thermoresponsive hydrogels is accomplished through a bifunctional polymeric network composed of hygroscopic zwitterionic moieties and thermoresponsive moieties. The ion immobilization within the zwitterionic segment yields confined hygroscopic sites, facilitating stable and advantageous water absorption across a range of RH levels. Concurrently, the incorporation of a thermoresponsive segment enables the release of water at comparatively low temperatures, underscoring the synergistic contribution of both the confined sites and the thermoresponsive network. Additionally, the microgel configuration endows the sorbent with rapid sorption–desorption kinetics. Results demonstrate that TZMG can achieve a water uptake of 1 g g^{-1} at 60% RH within 100 min and allow the release of approximately 80% of the captured water within 20 min at temperatures as low as 40 °C. Furthermore, by incorporating photothermal absorbers, solar-driven AWH can attain similar water release performance under one-sun illumination. With a comprehensively favorable performance, this research presents an effective and energy-efficient solution for the design of next-generation AWH sorbents, which holds potential to

alleviate the global water crisis at the materials level (Fig. 1*C* and *SI Appendix*, S2.2).

Results and Discussion

Characterization and Properties of Hydrogels. The thermo-responsive zwitterionic microgel (TZMG) proposed in this study is synthesized from a bifunctional copolymer, created through in situ free-radical polymerization of [2-(methacryloyloxy)ethyl] dimethyl-(3-sulfopropyl)ammonium hydroxide (DMAPS) and N-Isopropylacrylamide (NIPAM) monomers, followed by LiCl loading. The resulting ion-loaded P(NIPAM-co-DMAPS) network comprises two functional segments: a hygroscopic moiety, achieved through salt-immobilized PDMAPS with confined hygroscopic sites, and a thermoresponsive moiety, derived from PNIPAM (Fig. 2*A*). Initial examination of the synthesized polymeric hydrogel's fundamental properties employs Fourier transform infrared (FTIR) spectroscopy to analyze its chemical composition (Fig. 2*B*). For DMAPS, peaks at approximately 1,036 cm^{-1} and 1,178 cm^{-1} signify symmetric and asymmetric stretching vibrations of S=O, respectively. The characteristic peak at roughly 1,546 cm^{-1} corresponds to amide II in PNIPAM. The P(NIPAM-co-DMAPS) spectrum features a combination of these monomers' characteristic peaks, confirming successful copolymerization (31, 32). Moreover, X-ray diffraction (XRD) patterns of hydrogels, with a varying range of NIPAM:DMAPS copolymerization mole ratios from 1:0.1 to 1:1.0 after ion loading, display a broad peak around 20°, reflecting the amorphous nature of hydrogels, and lack distinct LiCl peaks. This observation implies that the majority of salt ions are present as ion pairs with zwitterions, rather than forming aggregated crystalline LiCl (Fig. 2*C*). To assess the salt-responsive property's influence on hydrogel swelling ability, the hydrogels are immersed in LiCl solution. A 4 M LiCl solution is selected as optimal for PDMAPS swelling (*SI Appendix*, S2.3). Fig. 2*D* illustrates the swelling ratio increase from ~0.5 g g^{-1} for PNIPAM to ~12 g g^{-1} for DMAPS. Electrostatic interactions cause self-association between zwitterionic groups of $-N^{+}(CH_3)_2-$ and $-SO_3^{-}$, which can be disrupted by Li^{+}/Cl^{-} ion pairing with zwitterions—a salting-in effect (33). Polymers frequently employed in AWH applications, like PNIPAM, typically experience a salting-out effect where their hydrability decreases in the presence of salt (34). Among the copolymer samples, the 1:1.0 copolymer hydrogel exhibits the highest swelling ability and potential water harvesting capacity, resulting from the competition between two salt-responsive properties. The phase transition behavior of the copolymer hydrogel is evaluated by monitoring the heat flow during temperature increase using differential scanning calorimetry (DSC). This phase transition is characterized by an endothermic peak in the DSC curve, representing the energy needed to disrupt polymer–solvent interactions and form a distinct polymer-rich phase (35, 36). The phase transition temperature shifts from ~34 °C for the 1:0.1 copolymer to ~39 °C for the 1:1.0 copolymer as the hydrophilicity is enhanced with more zwitterions incorporated (Fig. 2*E*). Although the transition degree notably decreases with greater DMAPS incorporation, it still significantly facilitates water release, as demonstrated in subsequent water desorption tests.

Preparation and AWH Performance of TZMGs. TZMGs are synthesized via the inverse miniemulsion polymerization method (37, 38) (Fig. 3*A*). Water-soluble monomers and crosslinkers undergo polymerization within surfactant-stabilized water-in-oil microdroplets, forming microgels. Upon completion of the ion impregnation process, the resultant TZMGs are obtained. Scanning electron microscopy (SEM) imaging reveals the as-prepared TZMGs possess dimensions of approximately 50 to 100 μm, with

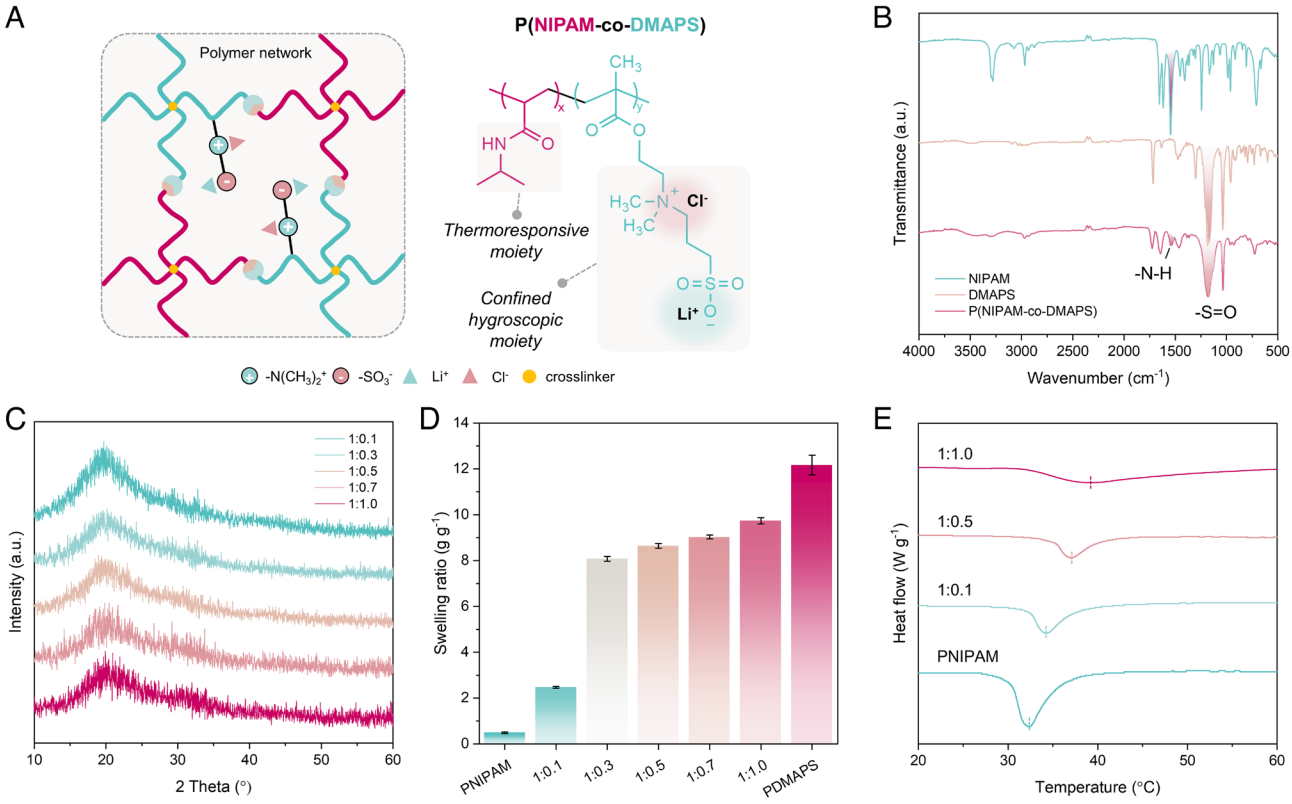

Fig. 2. Basic properties and characterization of copolymer hydrogels. (*A*) Schematic representation of copolymer structure and composition. (*B*) FT-IR spectra for monomers and copolymer. (*C*) XRD patterns of TZMG with varying copolymerization ratios. (*D*) Swelling ratios of hydrogels in 4 M LiCl solution. (*E*) Phase transition temperatures of hydrogels with different copolymerization ratios.

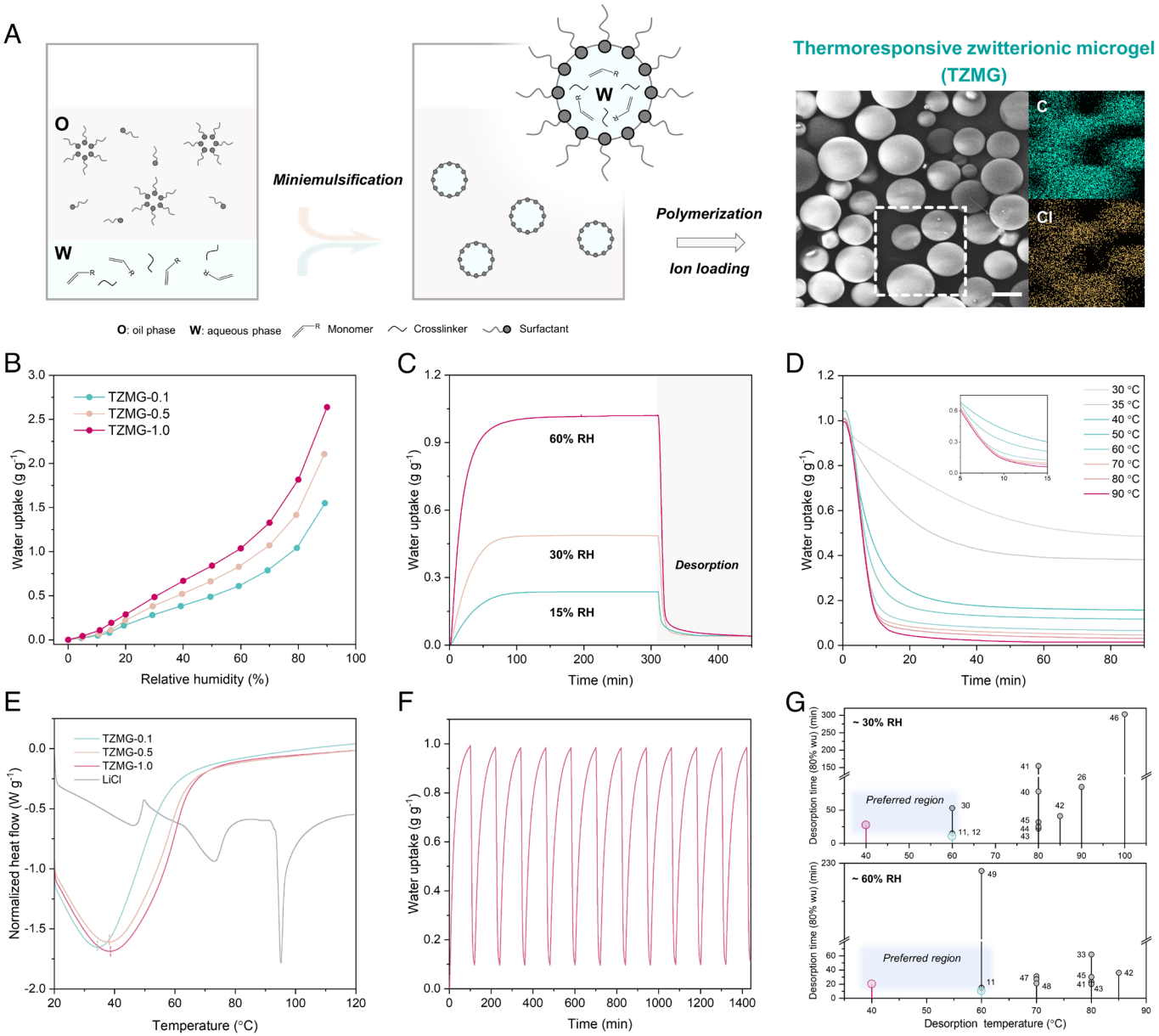

Fig. 3. AWH performance of TZMGs. (*A*) Schematic representation of the inverse mini-emulsion polymerization process, alongside SEM images and elemental mapping of as-prepared TZMG. (Scale bar: 50 μm.) (*B*) Water uptake of TZMGs at various RH levels. (*C*) Static water vapor sorption–desorption performance at different RH for TZMG-1.0. Sorption was conducted at 25 °C, while desorption took place at 60 °C. (*D*) Desorption curves for TZMG-1.0 at different temperatures. (*E*) Evaporation behavior of TZMGs and pure LiCl, hydrated with 1 g g^{-1} water uptake. (*F*) Cycling performance of TZMG-1.0, with sorption conditions set at 60% RH and a desorption temperature of 60 °C. For all tests, desorption occurred at a consistent water vapor pressure of 3.17 kPa. (*G*) Comparison plots of desorption performance of TZMG-1.0 with reported salt-contained/gel-based evaporation-based materials (11, 12, 26, 30, 33, 40–49). The fuchsia and turquoise dots refer to the desorption performance of this work.

uniformly distributed salt ions (*SI Appendix*, S2.5). The AWH properties of a series of TZMGs with varying copolymerization ratios are systematically examined. For conciseness, a TZMG with a NIPAM:DMAPS mole ratio of 1:0.1 is denoted as TZMG-0.1, and analogous nomenclature is used for others. Water vapor sorption isotherms are measured using a dynamic vapor sorption (DVS) system. Typically, the hygroscopic salt-driven moisture harvesting process exhibits a unique isotherm shape with three distinct phases: salt chemisorption, salt hydrate deliquescence, and subsequent salt solution absorption, wherein water uptake experiences a sudden increase at the deliquescence RH, as indicated by a slope change in isotherm (26, 29). Fig. 3*B* displays no abrupt inflection step in the isotherm, suggesting that the water capture mechanism is governed by confined hygroscopic sites rather than hygroscopic salt. The upward curve, alongside elevated RH, stems from hydrogel swelling caused by the increased water molecule mobility at high water activity (30, 39). Concurrently, TZMG-1.0 demonstrates the highest water uptake under various RH conditions due to the increased copolymerization of hygroscopic moieties. The water vapor sorption–desorption kinetics of TZMGs are evaluated through a static test. TZMGs with different copolymerization ratios exhibit similar sorption kinetics at 60% RH, achieving equilibrium (weight change rate ≈ 0 g g^{-1} min^{-1}) within approximately 100 min (*SI Appendix*, S2.6). Furthermore, the optimized TZMG exhibits a water uptake of 0.23 g g^{-1} at 15% RH and 0.48 g g^{-1} at 30% RH, verifying its applicability in low RH regions (Fig. 3*C*). The sorption time required to attain 80% of saturated water uptake at 15, 30, and 60% RH is 50, 45, and 30 min, respectively. Such rapid kinetics, resulting from the short diffusion distance of microgels, potentially enhance overall productivity through multiple cycling operations.

The captured water in TZMG-1.0 can be released by approximately 90% within 15 min through mild heating at 60 °C. Furthermore,

TZMG-1.0 can discharge over 80% of absorbed water within around 20 min at a relatively low temperature of 40 °C (Fig. 3*D* and *SI Appendix*, S2.7). The exceptional water release property is attained by incorporating thermoresponsive moieties into the copolymer network, whose conformational changes facilitate the escape of the confined water network, which is supported by both hydrophilic polymer chains and pendant hygroscopic groups. The impact of thermoresponsive properties on water release is substantiated through the comparison of desorption patterns both below and above the phase transition temperature, previously pinpointed to be ~39 °C. As depicted in Fig. 3*D*, TZMG-1.0 shows a progressive and slow decline in equilibrium uptake at 30 and 35 °C. This phenomenon is a result of increased molecular motion influenced by higher temperatures and reduced RH at a constant water pressure. It's crucial to note that this progressive decline in water uptake, while essentially a desorption process, is not directly tied to the phase transition but is linked to the specific thermodynamic conditions at play. As the system crosses the phase transition temperature, the thermoresponsive trait of the copolymer begins to dominate, leading to a significant surge in water desorption over a short time frame, underscoring the dominant role of the thermoresponsive behavior in the water release process. In comparison to conventional PNIPAM-LiCl-based sorbents, which predominantly rely on salt for moisture harvesting, TZMG-1.0 demonstrates its advantage in efficient water release at substantially lower temperatures. In the case of PNIPAM-LiCl, elevated thermal energy is requisite for decomposing salt hydrates, contributing to the desorption process (*SI Appendix*, S2.8). Conversely, the confined hygroscopicity and hydration of TZMG-1.0 enable efficient water release, underscoring the effectiveness of our proposed design. To gain a deeper understanding of the desorption process, the heat flow profiles of LiCl, TZMGs, PNIPAM-LiCl, and PDMAPS-LiCl are assessed using DSC. In Fig. 3*E*, the desorption process of the pristine LiCl solution, represented by the grey curve, displays three distinct evaporation peaks at approximately 46, 70, and 95 °C. These peaks correspond to the evaporation from the bulk solution, crystallization, and chemical desorption of LiCl, respectively (29, 30). Correspondingly, a typical hydrogel/salt composite, such as PNIPAM-LiCl, exhibits desorption peaks of salt hydrate and chemisorbed water in the heat flow profile, as discussed in *SI Appendix*, S2.9. In contrast to LiCl and PNIPAM-LiCl, TZMGs and PDMAPS-LiCl exhibit only a single primary evaporation peak, corroborating that the hygroscopicity source is dominated by the hydration of confined hygroscopic ion pairs rather than the deliquescence process of free crystalline LiCl. Moreover, the temperature at which major evaporation occurs increases from 32 °C for PNIPAM-LiCl to 34 °C for TZMG-0.1 and 39 °C for TZMG-1.0. This noticeable shift suggests that the incorporation of zwitterionic segments elevates the phase transition temperature, aligning with our previous experimental observations in Fig. 2*E* (*SI Appendix*, S2.10). Additionally, TZMG-1.0 can ideally and stably operate 12 cycles per day with 100-min harvesting and 20-min releasing at 60% RH (Fig. 3*F*). Given the broad operative RH range with competitive water uptake, rapid kinetics (*SI Appendix*, S2.11), and superior desorption behavior (Fig. 3*G* and *SI Appendix*, S2.12), the proposed TZMG has the potential to serve as an efficient AWH sorbent, exhibiting outstanding comprehensive performance.

Preparation and AWH Performance of PZMGs (Photothermal-Responsive Zwitterionic Microgels). By further incorporating photothermal absorbers, such as polypyrrole (Ppy), TZMG can be endowed with solar-driven water release capabilities. As the inverse miniemulsion polymerization method necessitates a homogeneous aqueous phase to generate stabilized emulsions, polypyrrole doped with polystyrene sulfonate (Ppy:PSS) is employed to form a water-processable solution (50) (Fig. 4*A* and *SI Appendix*, S2.13

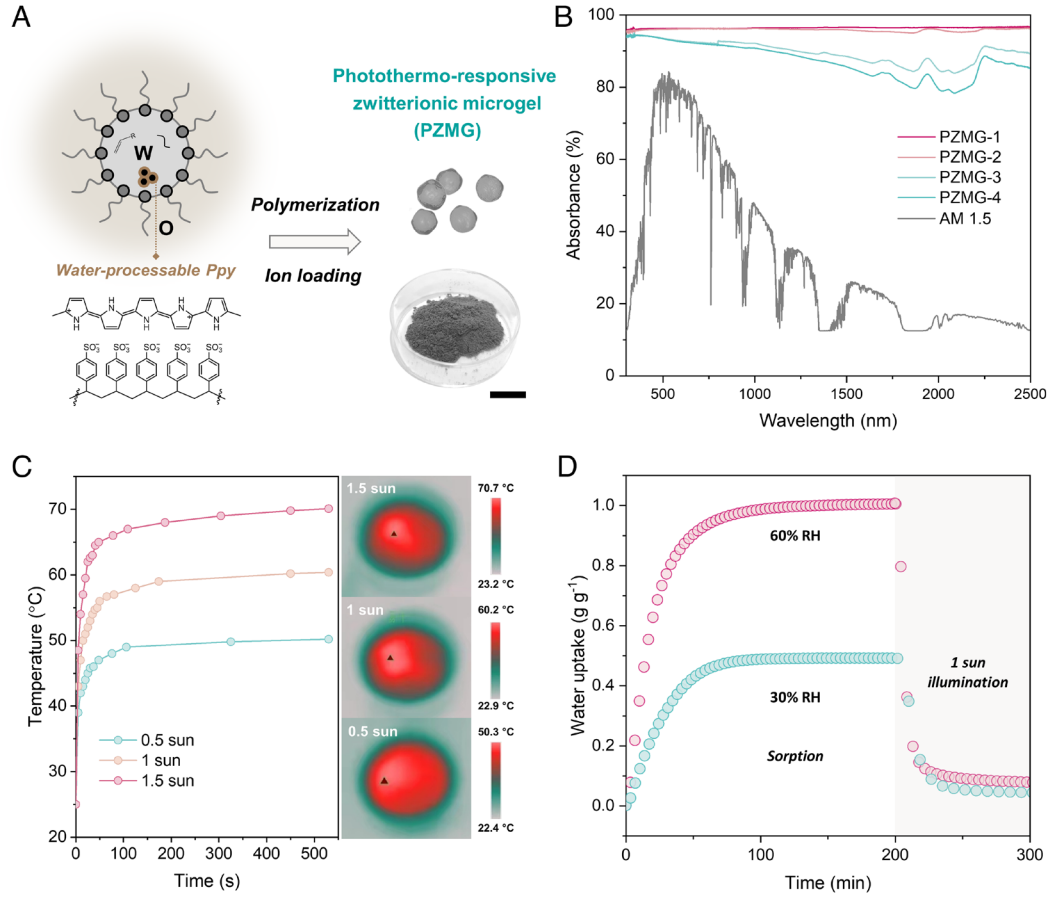

Fig. 4. Photothermal ability and solar-driven vapor sorption–desorption properties of PZMGs. (*A*) Schematic illustration of the PZMG synthesis process. (Scale bar: 1 cm.) (*B*) UV–Vis–NIR spectra of PZMGs with varying Ppy contents, and the normalized spectral solar irradiance density of air mass 1.5 global (AM 1.5 G) tilt solar spectrum. Specifically, PZMG 1 to 4 corresponds to PZMG with 15 vol%, 10 vol%, 5 vol%, and 2 vol% of 0.1 g/mL Ppy:PSS solution. (*C*) Time-dependent surface temperature and the IR thermal images of PZMG-1 under different light intensities. (*D*) Water vapor sorption curve under 60% RH and desorption curve under 1 sun of PZMG-1, and sorption–desorption rates (green dots) of PAMG-1.

and S2.14). Following a similar synthetic route to TZMGs with water-dispersed Ppy incorporated, PZMGs can be obtained. The as-prepared PZMGs exhibit a similar morphology to TZMG (*SI Appendix*, S2.15). PZMG-1, with an optimized Ppy:PSS solution included, demonstrates exceptional solar absorption (≈97%) over an extensive wavelength range from 250 to 2,500 nm (Fig. 4*B*). The photothermal properties of PZMG-1 are assessed by monitoring the surface temperature under varying solar intensities (Fig. 4*C* and *SI Appendix*, S1.1). The Ppy:PSS nanoparticles can attain heat confinement and efficient heating of the molecular mesh (*SI Appendix*, S2.16). As a result, the surface can reach equilibrium temperatures of approximately 50, 60, and 70 °C within 10 min under 0.5, 1, and 1.5 sun illumination (Fig. 4*C*). The favorable photothermal ability, combined with the relatively low regeneration temperature of the system, potentially enables solar-driven water release. The sorption-solar desorption properties of PZMG-1 are evaluated (Fig. 4*D*). Under conditions of 30% and 60% RH sorption and 1 sun illumination desorption, PZMG-1 exhibits similar kinetics and almost identical water uptake (~0.5 and 1 g g^{-1}, respectively) as TZMG-1.0, due to the minimal amount of added Ppy. Typically, 80% of absorbed water can be released within 20 min under 1 sun, indicating the feasibility of water release driven by natural sunlight.

The water extraction test is conducted using a homemade solar-driven AWH system to verify the viability of atmospheric water extraction (Fig. 5*A*). The AWH system comprises a transparent glass dome for light penetration and vapor condensation, a water collection base, and a sealing ring. A PZMG layer (~2 mm) is packed in a petri dish surrounded by thermal insulation foam. The samples undergo moisture sorption in a homemade moisture generation chamber at ~30% RH for 90 min and ~60% RH for 120 min (*SI Appendix*, S1.2), respectively, and experience water release under simulated solar light with 1 sun intensity for 30 min. As shown in Fig. 5*B*, the PZMG layer can absorb ~0.4 g g^{-1} and ~1.0 g g^{-1} water at 30% and 60% RH, respectively, and release most of it under sunlight. Additionally, batch cycling is performed. PZMG can stably operate at 60% RH over 10 cycles with an average water uptake of 0.99 g g^{-1}, water release of 0.92 g g^{-1}, and water collection of 0.70 g g^{-1} per cycle (Fig. 5*C*). It can also achieve an average water collection of 0.27 g g^{-1} per cycle at 30% RH (*SI Appendix*, S2.17). Furthermore, even after repeated cycling operations, the ions remain securely confined within the hydrogel matrix, demonstrating no obvious leakage or aggregation (*SI Appendix*, S2.18). Moreover, the concentrations of various metal ions in the collected water are significantly below the WHO standard (Fig. 5*D*). The results validate the freshwater delivery capability of PZMG. It should be noted that the yield and production efficiency can be further enhanced, as our demonstration is a proof-of-concept and not the best engineering practice. More effective active or passive cooling approaches can be adapted to increase the temperature difference between sorbents and the condensation surface, such as cooling fans or radiative cooling surfaces (7, 13, 51).

Conclusions

In conclusion, we have presented an approach to advanced sorbent design for AWH by implementing molecularly confined hydration in thermoresponsive hydrogels. The underlying design rationale enables the strategic manipulation of hygroscopicity and hydration

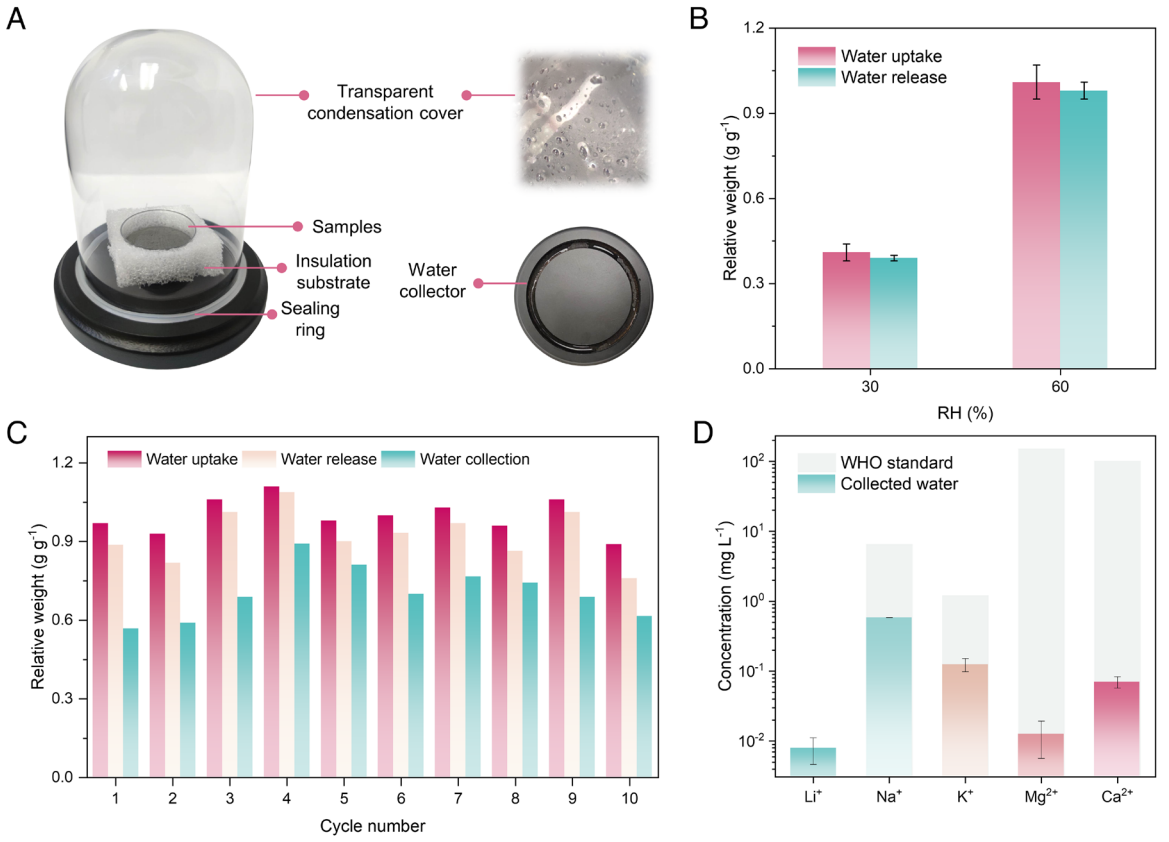

Fig. 5. Atmospheric water extraction. (*A*) Optical images of the homemade solar-driven AWH system. (*B*) Water uptake and release at different RH levels. (*C*) Cycling performance of PZMG at 60% RH. (*D*) Collected water quality assessed by ICP-MS. An estimated limit of 0.70 mg/L in drinking water was calculated by using a United States Environmental Protection Agency oral reference dose of 20 μg/kg/day (52).

through the synergistic interplay between confined ions and a thermoresponsive network. By utilizing a bifunctional polymeric network, which incorporates hygroscopic zwitterionic moieties alongside thermoresponsive constituents, we have achieved stable water uptake, efficient water release at a remarkably low temperature of 40 °C, one of the lowest reported values, and rapid sorption-desorption kinetics. Furthermore, the incorporation of photothermal absorbers enables solar-driven AWH, demonstrating comparable water release performance under natural sunlight. This work may provide an effective design of energy-efficient and high-performance AWH sorbents, which can contribute to addressing the global freshwater crisis at the materials level.

Materials and Methods

Fabrication of TZMGs. In a typical synthesis, a solution (A) was prepared by dissolving NIPAM, DMAPS, BIS (0.3 M), and APS (0.4 M) in water, with NIPAM fixed at 10 wt.% and NIPAM:DMAPS molar ratios varying between 1:0.1 and 1:1. Span 80 (0.025 vol%) was added to cyclohexane to form solution B. Solution A was purged with nitrogen for 15 min, combined with solution B (1:4 v/v ratio), and stirred, with TEMED (0.02 vol%) added after 30 and 60 min. After 24 h, the product was washed with cyclohexane, acetone, and water and then freeze-dried for 72 h. The resulting TZMG powder was immersed in 4 M LiCl for 24 h, washed, and freeze-dried again for 72 h.

Fabrication of Water-Dispersed Polypyrrole (Ppy:PSS). In a typical synthesis, in 0.1 M HCl, 0.27 g/mL polystyrene-sulfonate and 1.5 M ammonium persulfate were dissolved under N_2, and 20 g pyrrole was added. The reaction proceeded at 20 °C for 4 h, with the pH adjusted to 7.0. The polypyrrole–polystyrene sulfonate solution was dialyzed, freeze-dried, and redispersed in DI water to obtain a 0.1 g/mL Ppy solution.

Fabrication of PZMGs. In a typical synthesis, solution A was prepared similarly to TZMGs, with the extra addition of 0.1 g/mL Ppy:PSS (2, 5, 10, 15 vol%). The PZMG synthesis procedure was identical to that of TZMGs, yielding ion-loaded PZMG powder after freeze-drying.

Characterizations. Sample morphologies were observed using SEM and STEM (Hitachi S5500). FTIR spectra were collected using a Thermo Mattson Infinity Gold FTIR Spectrometer with a liquid nitrogen-cooled narrow-band mercury cadmium telluride detector and a Ge crystal ATR cell. XRD profiles were acquired with a Rigaku Miniflex 600 diffractometer. Thermogravimetric analysis was performed using a PerkinElmer TGA 4000 with an airflow rate of 25 mL min^{-1} and a heating rate of 10 °C min−1. Sorption–desorption performance was assessed using a Surface Measurement Systems DVS Adventure instrument, with samples preheated at 90 °C, 0% RH for 60 min, and stabilized at 25 °C for 30 min. Evaporation and phase transition behaviors were evaluated using a TA Instruments DSC 250 with a fixed scan rate of 2 °C min^{-1}. Ion concentrations were determined via ICP–MS (inductivelycoupled plasma mass spectrometry) (Agilent 7500ce). A dry, sealed cabinet containing desiccants was employed to prevent moisture sorption during sample transfer for characterization and performance measurements.

Data, Materials, and Software Availability. All study data are included in the article and/or *SI Appendix*.

ACKNOWLEDGMENTS. G.Y. acknowledges the financial support from the Welch Foundation Award F-1861, Norman Hackerman Award in Chemical Research, and Camille-Dreyfus Teacher-Scholar Award.

1. World Health Organization & United Nations Children's Fund (UNICEF), Progress on drinking water, Sanitation and hygiene: 2017 update and SDG baselines (World Health Organization and the United Nations Children's Fund, 2017).
2. M. M. Mekonnen, A. Y. Hoekstra, Four billion people facing severe water scarcity. *Sci. Adv.* **2**, e1500323 (2016).
3. J. Lord *et al.*, Global potential for harvesting drinking water from air using solar energy. *Nature* **598**, 611–617 (2021).
4. T. Oki, S. Kanae, Global hydrological cycles and world water resources. *Science* **313**, 1068–1072 (2006).
5. F. Fathieh *et al.*, Practical water production from desert air. *Sci. Adv.* **4**, eaat3198 (2018).
6. N. Hanikel, M. S. Prévot, O. M. Yaghi, MOF water harvesters. *Nat. Nanotechnol.* **15**, 348–355 (2020).
7. A. LaPotin, H. Kim, S. R. Rao, E. N. Wang, Adsorption-based atmospheric water harvesting: Impact of material and component properties on system-level performance. *Acc. Chem. Res.* **52**, 1588–1597 (2019).
8. M. Ejeian, R. Z. Wang, Adsorption-based atmospheric water harvesting. *Joule* **5**, 1678–1703 (2021).
9. A. LaPotin *et al.*, Dual-stage atmospheric water harvesting device for scalable solar-driven water production. *Joule* **5**, 166–182 (2021).
10. H. Lu *et al.*, Materials engineering for atmospheric water harvesting: Progress and perspectives. *Adv. Mater.* **34**, 2110079 (2022).
11. Y. Guo *et al.*, Scalable super hygroscopic polymer films for sustainable moisture harvesting in arid environments. *Nat. Commun.* **13**, 2761 (2022).
12. W. Guan, C. Lei, Y. Guo, W. Shi, G. Yu, Hygroscopic-microgels-enabled rapid water extraction from arid air. *Adv. Mater.* **35**, 2207786 (2022).
13. Y. Song *et al.*, High-yield solar-driven atmospheric water harvesting of metal–organic-framework-derived nanoporous carbon with fast-diffusion water channels. *Nat. Nanotechnol.* **17**, 857–863 (2022).
14. X. Zhou, H. Lu, F. Zhao, G. Yu, Atmospheric water harvesting: A review of material and structural designs. *ACS Mater. Lett.* **2**, 671–684 (2020).
15. W. Shi, W. Guan, C. Lei, G. Yu, Sorbents for atmospheric water harvesting: From design principles to applications. *Angew. Chem. Int. Ed. Engl.* **61**, e202211267 (2022).
16. Y. Guo *et al.*, Hydrogels and hydrogel-derived materials for energy and water sustainability. *Chem. Rev.* **120**, 7642–7707 (2020).
17. F. Zhao *et al.*, Super moisture-absorbent gels for all-weather atmospheric water harvesting. *Adv. Mater.* **31**, 1806446 (2019).
18. R. Li *et al.*, Hybrid hydrogel with high water vapor harvesting capacity for deployable solar-driven atmospheric water generator. *Environ. Sci. Technol.* **52**, 11367–11377 (2018).
19. D. Roy, W. L. A. Brooks, B. S. Sumerlin, New directions in thermoresponsive polymers. *Chem. Soc. Rev.* **42**, 7214–7243 (2013).
20. M. A. C. Stuart *et al.*, Emerging applications of stimuli-responsive polymer materials. *Nat. Mater.* **9**, 101–113 (2010).
21. H. G. Schild, Poly(N-isopropylacrylamide): Experiment, theory and application. *Prog. Polym. Sci.* **17**, 163–249 (1992).
22. M. Heskins, J. E. Guillet, Solution properties of Poly(N-isopropylacrylamide). *J. Macromol. Sci.* **2**, 1441–1455 (1968).
23. G. Yilmaz *et al.*, Autonomous atmospheric water seeping MOF matrix. *Sci. Adv.* **6**, eabc8605 (2020).
24. K. Matsumoto, N. Sakikawa, T. Miyata, Thermo-responsive gels that absorb moisture and ooze water. *Nat. Commun.* **9**, 2315 (2018).
25. X. Chang *et al.*, Marine biomass-derived, hygroscopic and temperature-responsive hydrogel beads for atmospheric water harvesting and solar-powered irrigation. *J. Mater. Chem.* **10**, 18170–18184 (2022).
26. J. Xu *et al.*, Ultrahigh solar-driven atmospheric water production enabled by scalable rapid-cycling water harvester with vertically aligned nanocomposite sorbent. *Energy Environ. Sci.* **14**, 5979–5994 (2021).
27. B. Kang, H. Tang, Z. Zhao, S. Song, Hofmeister series: Insights of ion specificity from amphiphilic assembly and interface property. *ACS Omega* **5**, 6229–6239 (2020).
28. M. Hua *et al.*, Strong tough hydrogels via the synergy of freeze-casting and salting out. *Nature* **590**, 594–599 (2021).
29. J. Xu *et al.*, Efficient solar-driven water harvesting from arid air with metal-organic frameworks modified by hygroscopic salt. *Angew. Chem. Int. Ed. Engl.* **59**, 5202–5210 (2020).
30. H. Lu *et al.*, Tailoring the desorption behavior of hygroscopic gels for atmospheric water harvesting in arid climates. *Adv. Mater.* **34**, 2205344 (2022).
31. Z. Lei, P. Wu, A highly transparent and ultra-stretchable conductor with stable conductivity during large deformation. *Nat. Commun.* **10**, 3429 (2019).
32. Y. Shi, C. Ma, L. Peng, G. Yu, Conductive "smart" hybrid hydrogels with PNIPAM and nanostructured conductive polymers. *Adv. Funct. Mater.* **25**, 1219–1225 (2015).
33. S. Aleid *et al.*, Salting-in effect of zwitterionic polymer hydrogel facilitates atmospheric water harvesting. *ACS Mater. Lett.* **4**, 511–520 (2022).
34. Y. Zhang, S. Furyk, D. E. Bergbreiter, P. S. Cremer, Specific ion effects on the water solubility of macromolecules: PNIPAM and the hofmeister series. *J. Am. Chem. Soc.* **127**, 14505–14510 (2005).
35. I. Shechter, O. Ramon, I. Portnaya, Y. Paz, Y. D. Livney, Microcalorimetric study of the effects of a chaotropic salt, KSCN, on the lower critical solution temperature (LCST) of aqueous Poly(N-isopropylacrylamide) (PNIPA) solutions. *Macromolecules* **43**, 480–487 (2010).
36. H. Feil, Y. H. Bae, J. Feijen, S. W. Kim, Effect of comonomer hydrophilicity and ionization on the lower critical solution temperature of N-isopropylacrylamide copolymers. *Macromolecules* **26**, 2496–2500 (1993).
37. I. Capek, On inverse miniemulsion polymerization of conventional water-soluble monomers. *Adv. Colloid Interface Sci.* **156**, 35–61 (2010).
38. T. Kietzke *et al.*, Novel approaches to polymer blends based on polymer nanoparticles. *Nat. Mater.* **2**, 408–412 (2003).
39. H. Mittal, A. Al Alili, S. M. Alhassan, Adsorption isotherm and kinetics of water vapors on novel superporous hydrogel composites. *Microporous Mesoporous Mater.* **299**, 110106 (2020).
40. C. Lei *et al.*, Polyzwitterionic hydrogels for efficient atmospheric water harvesting. *Angew. Chem. Int. Ed. Engl.* **61**, e202200271 (2022).
41. A. Entezari, M. Ejeian, R. Wang, Super atmospheric water harvesting hydrogel with alginate chains modified with binary salts. *ACS Mater. Lett.* **2**, 471–477 (2020).
42. R. Li, Y. Shi, M. Wu, S. Hong, P. Wang, Photovoltaic panel cooling by atmospheric water sorption–evaporation cycle. *Nat. Sustain.* **3**, 636–643 (2020).
43. F. Deng, C. Wang, C. Xiang, R. Wang, Bioinspired topological design of super hygroscopic complex for cost-effective atmospheric water harvesting. *Nano Energy* **90**, 106642 (2021).
44. F. Deng, C. Xiang, C. Wang, R. Wang, Sorption-tree with scalable hygroscopic adsorbent-leaves for water harvesting. *J. Mater. Chem.* **10**, 6576–6586 (2022).
45. R. Li, Y. Shi, M. Wu, S. Hong, P. Wang, Improving atmospheric water production yield: Enabling multiple water harvesting cycles with nano sorbent. *Nano Energy* **67**, 104255 (2020).
46. P. A. Kallenberger, M. Fröba, Water harvesting from air with a hygroscopic salt in a hydrogel–derived matrix. *Commun. Chem.* **1**, 28 (2018).

47. M. Wu *et al.*, Metal- and halide-free, solid-state polymeric water vapor sorbents for efficient water-sorption-driven cooling and atmospheric water harvesting. *Mater. Horizons* **8**, 1518–1527 (2021).
48. K. Yang *et al.*, Hollow spherical SiO2 micro-container encapsulation of LiCl for high-performance simultaneous heat reallocation and seawater desalination. *J. Mater. Chem.* **8**, 1887–1895 (2020).
49. J. Wang *et al.*, High-yield and scalable water harvesting of honeycomb hygroscopic polymer driven by natural sunlight. *Cell Rep. Phys. Sci.* **3**, 100954 (2022).
50. G. Markham, T. M. Obey, B. Vincent, The preparation and properties of dispersions of electrically-conducting polypyrrole particles. *Colloids Surf.* **51**, 239–253 (1990).
51. I. Haechler *et al.*, Exploiting radiative cooling for uninterrupted 24-hour water harvesting from the atmosphere. *Sci. Adv.* **7**, eabf3978 (2021).
52. D. G. Barnes, M. Dourson, Reference dose (RfD): Description and use in health risk assessments. *Regul. Toxicol. Pharmacol.* **8**, 471–486 (1988).